Furnace Tapping 2018, Edited by J.D. Steenkamp & A. Cowey,
Southern African Institute of Mining and Metallurgy, Kruger National Park, 14–17 October 2018

Reduced metal loss to slag in HC FeCr production – by redesign based on mathematical modelling

S.T. Johansen[1,2] and E. Ringdalen[1]

[1]SINTEF Industry
[2]NTNU, Norway

We describe a case from HCFeCr production where redesign of the tapping configuration resulted in a considerable reduction in metal losses to tapped slag. The redesign was based on mathematical modelling of the flow of tapped slag and 3D computational fluid dynamics.

Keywords: Tapping jet, slag, metal loss, heat loss, droplet breakup, separation.

INTRODUCTION

At the ferrochromium plant at Mo i Rana, Norway, significant loss of metal to the slag was experienced after a redesign of the tapping area in 1997. The loss was substantially larger than anticipated.

It was decided to initiate a study of the phenomena involved in the metal loss. Factors like tapping rate, the velocity of the metal along its path from the furnace to the ladle, slag viscosity, temperature distribution, and geometrical configuration of the primary ladle were investigated in some detail. The physical phenomena at play were studied by means of computational fluid dynamics (CFD), using commercial software.

In this paper we describe the physical phenomena and explain how a combination of physical insight and rather simplistic flow simulations can be applied to analyse a critical industrial problem. We further explain the results of the study and discuss some generic guidelines for minimizing metal loss to a slag phase.

The recommendations from the study led to a second redesign of the tapping area, after which the in-plant metal loss to the slag was substantially reduced.

MODEL DEVELOPMENT

The Industrial Challenge

In 1997 the Elkem Mo i Rana Ferrochromium furnace was redesigned during a furnace reline. At the same time some modifications of the tapping area were introduced. Shortly afterwards a significant increase in metal loss to the slag phase was observed. As it was not clear what the causes of this were, SINTEF was asked to contribute to resolving the issue.

A Systematic Approach to Problem-solving

Recently, SINTEF has developed a systematic approach to resolving industrial challenges. This approach, named 'Pragmatic Industrial Modelling' (Zoric *et al*., 2014, 2015; Johansen *et al*., 2017) focuses on the industrial requirements for a model. Fundamental to 'Pragmatic Modelling' (in short) is that the modelling work should focus on solving the industrial challenge. According to the Pragmatic Modelling concept,

the work must be based on finding a solution quickly, within the set industrial time and cost frames. In fact, the development of the Pragmatic Modelling concept was borne out of many projects carried out in collaboration with industry. In particular, several important contributions to Pragmatic Modelling were developed during this work, which had its origins back in 1998 but has more recently been generalized by the papers referenced above.

The development project started out with a meeting in 1998 at the Mo i Rana plant, where representatives from SINTEF and Elkem discussed the changes in metal yield, as well as the geometrical and operational changes introduced though the retrofit. A major purpose in this meeting was to ensure that all participants had a common understanding of the problem.

First Observations and Working Hypothesis

Observations around the operating furnace and outdoor revealed several important physical phenomena. The tapping arrangement is depicted in Figure 1.

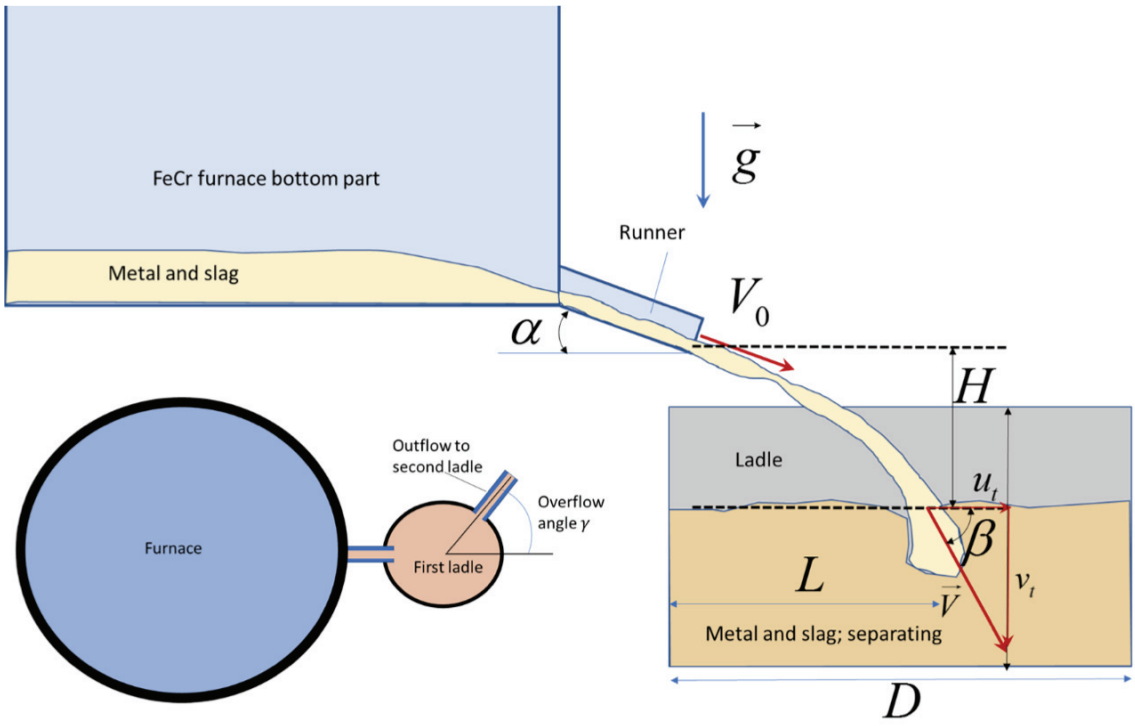

Figure 1. Configuration of the tapping arrangement. Insert in lower left shows a plan view of the tapping arrangement.

The tapping rate is controlled by several phenomena and can today be understood in some detail (Kadkhodabeigi, Tveit, and Johansen, 2010). Modelling for this case had to be based on the knowledge at the time, but more recent knowledge is also included in parts of the discussion. For the actual modelling work the tapping rate was assumed from previous taps, based on tapping time and registered tapped masses of metal and slag. The tapping stream, after leaving the runner (Figure 1) may partially break up into smaller droplets (Berg *et al.*, 1999; Laux *et al.*, 2000). When the jet splashes onto the liquid surface in the ladle the jet will penetrate into the liquid below, entraining gas bubbles into the liquid. In addition, the high shear stress at the perimeter of the penetrating jet will shed off metal droplets from the jet, or break up previous metal droplets in the vicinity of the jet. The larger metal droplets will settle to the bottom of the ladle, until the surface of the metal-continuous layer is reached. As a result, the slag phase, which has the lower density, will accumulate in the upper part of the ladle. The viscosity of the slag phase varies strongly with temperature, and may become considerable if the

temperature drops. Ferrochromium slag also contains solid particles of unreduced ore and precipitates, which contribute to the high viscosity. An increased slag viscosity would in the next stage lead to reduced droplet settling and thereby poorer slag-metal separation. When the first ladle is almost full, the slag overflows into a second ladle (slag ladle) through an overflow runner. Metal droplets that were transported by the slag flowing over into the slag ladle were considered as lost.

As of result of these general considerations, the metal yield was expected to deteriorate if the droplet size was reduced or the slag viscosity was increased.

The tapping configuration had been redesigned as a part of a project to increase efficiency and the health, environmental, and safety (HES) conditions in the plant. Referring to Figure 1, the following modifications were performed during the furnace reline, which contributed to the poor slag and metal separation. First, the length and inclination, α, of the runner had been increased. Also, the vertical distance from the end of the runner to the liquid surface, *H*, was increased. Because of these modifications, the liquid velocity at the impingement point, at the surface of the ladle, was increased. In addition, the position where the liquid stream impacted on the liquid surface, *L,* was shifted so that it was much closer to the overflow runner.

We may note that the liquid velocity in the runner may be approximated as steady state. In this case the liquid velocity out of the runner may be approximated by accounting for the effects of gravity and friction against the runner.

Theoretical Considerations

It is well known that for an inclined open channel flow the velocity may be estimated by:

$$V_0 = \left(\frac{8g \sin \alpha}{f} R_h \right)^{\frac{1}{2}} \qquad [1]$$

Based on the velocity V_0 (see Figure 1), the observed tapping rate, and runner cross-sectional geometry, we can calculate the liquid level and the velocity in the runner. As the liquid level enters the hydraulic radius in Equation [1], a few iterations are needed to obtain the velocity and runner liquid level. Based on the runner inclination angle α and V_0 we use Newtonian kinetics to calculate the trajectory of the metal jet from the runner. The effects of friction with air and liquid break-up are neglected here. The liquid will move with constant horizontal velocity $V_H = V_0 \cos(\alpha)$ out from the runner, and with vertical downward velocity $V_V = V_0 \cos(\alpha) + gt$, where *t* is the time from when the metal exits the runner.

The heat loss from the metal on its way along the runner must be assessed. A simple heat balance may be estimated from:

$$\dot{m} c_p (T_2 - T_1) = -\dot{q}_w A_w - \sigma_{SB} f(\varepsilon) \left(\overline{T}^4 - T_\infty^4 \right) \qquad [2]$$

Here, m is the liquid mass flow rate, c_p is the liquid heat capacity, T_1 and T_2 are the liquid entry and exit temperatures, q_w is the heat flux into the refractory, A_w is the wetted runner area, σ_{SF} is the Stefan-Boltzmann constant, $f(\varepsilon)$ is a combined

emissivity and view factor, $\bar{T} \approx \frac{T_1 + T_2}{2}$ is a rough approximation of the average surface temperature, and T_∞ is the far field temperature (approx. 20°C). The convective heat flux q_w between liquid and refractory in the runner can be approximated by

$$\dot{q}_w = \frac{\bar{T} - T_w}{T^+} \rho c_p u_\tau \qquad [3]$$

where T_w is the surface temperature of the refractory, and T^+ is the non-dimensional temperature, which is a function of the Prandtl number, the surface roughness, the liquid depth, the kinematic viscosity of the liquid, and the wall shear velocity $u_\tau = \sqrt{\frac{\tau_w}{\rho}}$ (Johansen, 1990; Ashrafian and Johansen, 2007). The resulting temperature loss in the runner was approximately 7 K.

Based on the information above it was possible to estimate the position and velocity of the tapping jet when it enters the top surface in the ladle.

If we consider metal droplets in a viscous slag phase, the settling velocity can be expressed by

$$V_t = \frac{(\rho_m - \rho_s) g d_d^{\,2}}{18 \mu_s} \left(\frac{C_D 24}{\mathrm{Re}_d} \right) \qquad [4]$$

In Equation [4] the droplet Reynolds number is given by $\mathrm{Re}_d = \frac{\rho_s d_d V_t}{\mu_s}$, and the drag function C_D is taken from Morsi and Alexander (1972). For the smaller droplets, having $d_d < \left(\frac{18 \mu_s^{\,2}}{\rho_s (\rho_m - \rho_s) g} \right)^{\frac{1}{3}}$, we can approximate by $\left(\frac{C_D 24}{\mathrm{Re}_d} \right) = 1$. Assuming slag density $\rho_s = 2700$ kg/m^3 and metal density $\rho_m = 6700$ kg/m^3, we present droplet settling velocities in Figure 2. As seen, the effect of viscosity is large, with the settling velocity inversely proportional to the slag viscosity.

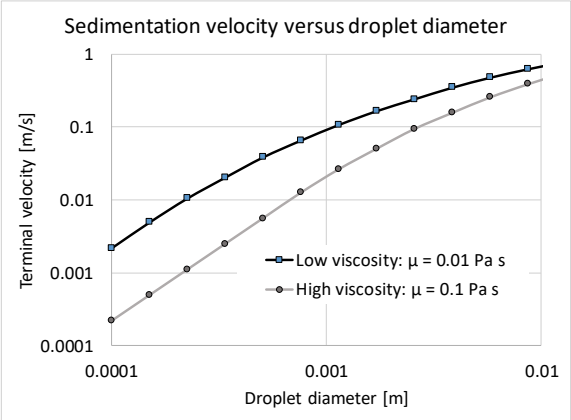

Figure 2. Metal droplet terminal velocities versus droplet size (high and low slag viscosity).

Estimation of Droplet Size

In turbulent flows, a representative droplet size may be estimated by the model from (Hinze, 1955):

$$d_d = 0.2\left(\frac{\sigma}{\rho}\right)^{0.6} \varepsilon^{-0.4} \qquad [5]$$

The turbulent dissipation rate ε was based on the flow along the primary runner, where a wall roughness of 3 mm for the refractory was applied. The resulting dissipation rate for the runner was estimated to be

$$\varepsilon = 1.75[m^{-1}] \cdot V^3 \qquad [6]$$

Below, we will see that by using flow simulations it is possible to directly compute the volume-averaged dissipation in a volume located around the impact zone of the tapping jet. Based on an obtained dissipation rate of $\varepsilon_0 = 10.0\ m^2/s^3$, from one simulation with low fall height *H* and impact velocity V_0 , the dissipation rate for higher fall heights were estimated by:

$$\varepsilon = \varepsilon_0 \cdot \left(\frac{V}{V_0}\right)^3 \qquad [7]$$

Based on these assessments, the typical droplet sizes were estimated and are presented in Table I. The free-fall heights refer to Table II. The estimates were based on Equations [5]–[7].

Table I. Estimated, typical droplet sizes, for the two main free-fall height scenarios.

	Runner	Impact zone	
		Fall height *L* = 0.15 m	Fall height *L* = 1.0 m
Droplet diameter d_d (mm)	0.53	0.70	0.25

CFD Simulations

Computational fluid dynamics (CFD) was selected as the best method to investigate the different flow situations. Based on our working hypotheses, we wanted to study the difference between the previous tapping arrangement (Furnace 1) and the new arrangement (Furnace 2). The main difference between the arrangements was the metal fall height *L*. In addition, the impact of differences in slag viscosity, slag flow rates, and the overflow angle γ were investigated. The different cases are given in Table II. We may note that for the different combinations of slag jet fall height *L*, slag viscosity, and slag flow rate, the impingement point (at slag top surface in the ladle) and slag jet velocity components will vary, as given by the equations above.

It was decided that the inflowing liquid could be modelled as a slag phase, and where the metal was dispersed into the slag, as droplets with a range of sizes.

The simulations were performed using the commercial software Fluent, version 4.47. Based on given geometrical information from the plant operation a numerical grid was designed. The grid was boundary-fitted to the geometry. The numerical method applied

Cartesian velocity vectors, using co-located grids (all fields stored at the same position, centrally in each grid cell). Two numerical grids were tested. However, it was found that the coarsest grid had sufficient resolution as the grid dependency was minor.

Table II. Overview of simulated flow cases.

Case ID	Furnace no.	Slag jet fall height H (m)	Slag viscosity (Pa s)	Slag flow rate (m^3/h)	Overflow angle γ
O1VQ1A0	1	0.15	0.01	33.2	0
O1VQ1A6	1	0.15	0.01	33.2	60
O1KQ1A0	1	0.15	0.1	33.2	0
O1KQ1A6	1	0.15	0.1	33.2	60
O2VQ1A0	2	1.0	0.01	33.2	0
O2VQ1A6	2	1.0	0.01	33.2	60
O2KQ1A0	2	1.0	0.1	33.2	0
O2KQ1A6	2	1.0	0.1	33.2	60

The ladle was in all cases assumed to be filled with slag and metal. The diameter of the jet impinging on the surface, the jet inflow velocity, inflow temperature, and the position of the jet inflow were all computed based on the methods and equations discussed above. Possible entrainment of gas around the jet perimeter was ignored, as it was considered not necessary to assess the relative importance or the case parameters. It was assumed that the temperature of the stream issuing from the tap-hole was a constant 1600°C. Only the heat loss in the runner was included in determining the inflow temperature. The free surface at the top was assumed to be an adiabatic and shear-free wall. The temperature of the refractory was set to 500°C. This was a crude first assumption.

The turbulence modelling was performed using the classical $k-\varepsilon$ model (Launder and Spalding, 1972), using classical wall-functions for wall boundary conditions for velocity and turbulence fields. In the incoming jet it was assumed that the turbulent intensity was 30% and the turbulent length scale was fixed to 20 mm. This corresponds to a highly turbulent incoming jet of liquid.

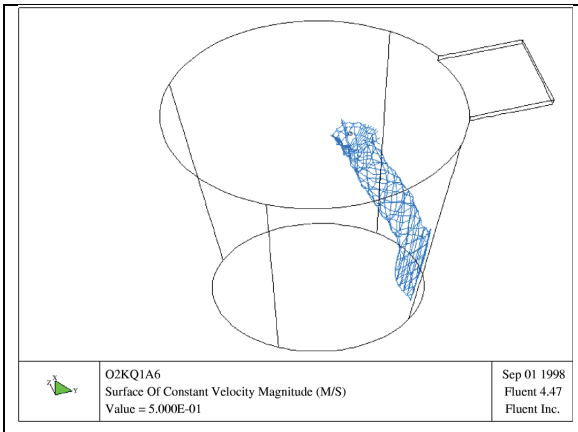

Figure 3. Iso-surface of slag velocity magnitude (U=0.5 m/s) for case Q2KQ1A6.

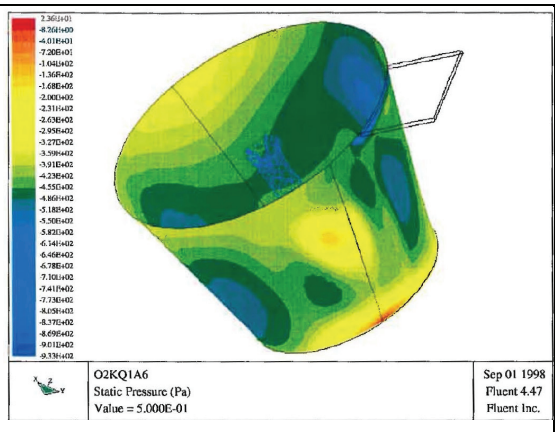

Figure 4. Pressure contours at refractory for case Q2KQ1A6.

Figure 3 depicts the slag flow induced in the ladle by the impinging tapping jet. The jet hits the refractory wall (where it may cause local erosion) and we realize that there may be quite extensive mixing inside the ladle. Figure 4 shows the predicted surface pressure (hydrostatic pressure effects are not included). The maximum pressures are located in

the jet stagnation areas. The pressure variations illustrate the strong flows throughout the ladle.

The metal droplets were simulated using turbulent Lagrangian tracking (Johansen and Boysan, 1988) of the droplets. Metal droplets that impinge on the ladle refractory wall were assumed trapped. At the top (free) surface the droplets would bounce. Droplets that left together with the overflow were assumed to have escaped. In Figure 5 we see an example where, out of three calculated droplets, two are trapped at the ladle wall, while one is escaping through the overflow.

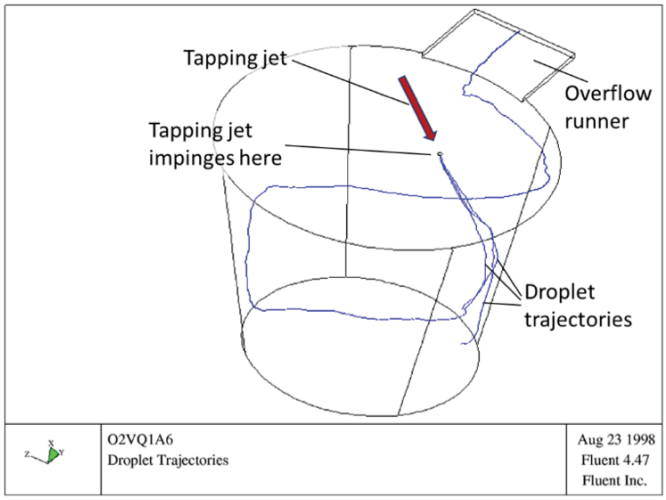

Figure 5. Predicted turbulent trajectories of three equally sized slag droplets. The flow case is Q2VQ1A6.

Simulation Results

In Figures 6 and 7 we see the predicted metal losses to overflow. We note that the impact of slag viscosity is very strong. For 400 μm diameter droplets there is no loss in the case of low slag viscosity (0.01 Pa.s), while there is 2–6% loss for high slag viscosity (0.1 Pa.s). We can also see that the impact of the tapping jet fall height (O1* = small *L*, O2* = large *L*) is substantial, as the metal level is higher for the cases with large *L* and same overflow angle (*A0 and *A6). In addition, for the cases with a large *L*, the tapping jet impinges at a much higher velocity, breaking up droplets and generating significant quantities of fine droplets. Hence, the actual effect is expected to be significantly stronger than seen in the simulation.

The final parameter to assess is γ, the angle of the overflow. We see from Figure 7 that the *A6 cases are better than the *A0 cases. The reason is that in the *A0 cases the metal impinges on the slag surface very close to the overflow. This results in strong flows close to the overflow and short-circuiting of metal droplets.

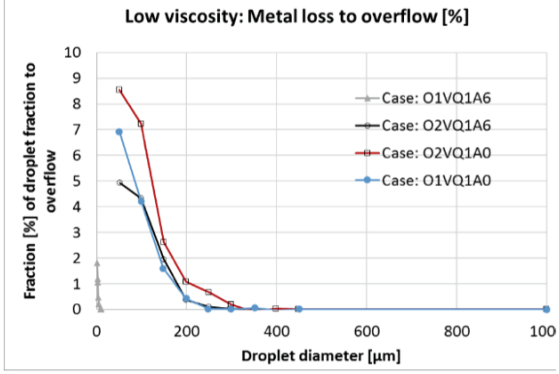

Figure 6. Low slag viscosity. Predicted metal loss to overflow versus metal droplet diameter.

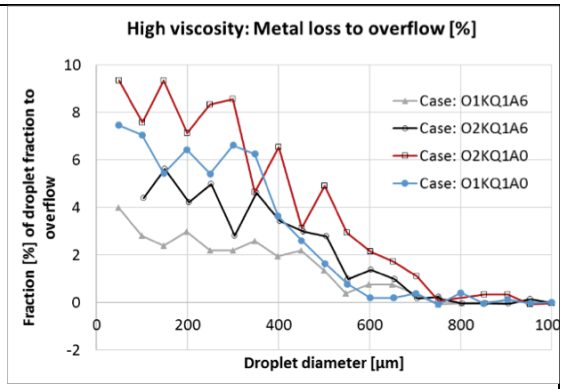

Figure 7. High slag viscosity. Predicted metal loss to overflow versus metal droplet diameter.

CONCLUSIONS

Based on the simulation results, it was calculated that the metal loss could be reduced by a factor of 30 by reducing the fall height from the end of the furnace runner to the liquid surface in the ladle. This was based on the estimated droplet sizes for the two cases and that the overflow runner was aligned straight forward (angle γ=0°). Extra metal loss caused by the metal trajectory at large fall height could be reduced by changing the overflow runner angle to γ=60°, reducing short-circuiting of droplets to the overflow. The metal loss to the overflow was estimated to be 200 times larger in the case of high viscosity. It would therefore be critical to reduce the heat losses from the slag/metal system in order to promote separation.

It was decided to rebuild the tapping area at the Mo i Rana FeCr plant. The liquid jet fall height and impingement velocity were minimized. The overflow runner was changed to position γ=60°, and actions were taken to reduce the heat loss from the top surface of the first ladle to maintain a high slag temperature and low slag viscosity.

As a result of these modifications the metal loss to the slag was substantially reduced. This work is considered as an excellent example of the application of CFD to solve industrial challenges. The concepts of 'Pragmatic Industrial Modelling' were applied in this work, in which CFD and knowledge of numerical methods, flow physics, and industrial understanding were all important elements of the applied toolbox.

ACKNOWLEDGEMENTS

Our former colleague Knut H. Bech is acknowledged for performing the CFD simulations. The NRC-supported project 267621 Controlled Tapping is acknowledged for financial support for preparing this publication.

LIST OF SYMBOLS

A_w Wall area (m^2)

c_p Heat capacity (JK^{-1})

C_D Drag coefficient (-)

D Inner diameter of ladle (m)

d Droplet diameter (m)

f Friction factor (-)

g Gravitational constant of (m/s^2)

H Free-fall height from end of runner to ladle free surface (m)

m Mass flow rate (kg/s)

R_h Hydraulic radius of runner (m/s)

q_w Wall heat flux (Wm^{-2})

s Wall roughness (m)

T Temperature (°K)

T^+ Dimensionless boundary layer temperature profile:

$$T^+\left(y^+, s^+\right) \equiv (T(y,s) - T_w) \cdot \rho c_p u_\tau / q_w$$

u_τ Wall shear velocity (m/s): $u_\tau = \sqrt{\tau_w / \rho}$

V_0 Velocity out of runner, or reference velocity (m/s)

V_t Settling velocity (m/s)

V Jet impact velocity on ladle free surface (m/s)

y Wall distance (m)

y^+ Dimensionless wall distance: $y^+ = \dfrac{y u_\tau}{\nu}$

Greek letters

α Runner inclination angle (º)

γ Overflow runner angle (Figure 1) (º)

τ_w Wall shear stress (Pa)

μ Viscosity (Pa.s)

ν Kinematic viscosity (m^2/s): $\nu = \mu / \rho$

σ Surface tension (Nm^{-1})

ρ Density (kg/m^3)

ε Turbulent dissipation rate (m^2/s^3)

Subscripts

m Metal

s Slag

d Droplet

w Wall

Other symbols

O1* All cases in Table II , case name starting with O1

O2* All cases in Table II , case name starting with O2

*A0 All cases in Table II , case name ending with A0

*A6 All cases in Table II , case name ending with A6

$\propto$ Refers to far field, or bulk flow

REFERENCES

Ashrafian, A. and Johansen, S.T. 2007. Wall boundary conditions for rough walls. *Progress in Computational Fluid Dynamics*, 7, 230–236.

Berg, H., Laux, H., Johansen, S.T., and Klevan, O.S. 1999. Flow pattern and alloy dissolution during tapping of steel furnaces. *Ironmaking & Steelmaking*, 26, 127–139. https://doi.org/10.1179/030192399677013

Hinze, J.O. 1955. Fundamentals of the hydrodynamic mechanism of splitting in dispersion processes. *AIChE Journal*, 1, 289–295.

Zoric, J., Busch, A., Meese, E.A., Khatibi, M., Time, R.W., S.T. Johansen, H., and Rabenjafimanantsoa, A.. 2015. On pragmatism in industrial modeling - Part II: Workflows and associated data and metadata. *Proceedings of the 11th International Conference on CFD in the Minerals and Process Industries,* Melbourne, Australia, 7-9 December 2015. Solnordal, C.B., Liovic, P., Delaney, G.W., Cummins, S.J., Schwarz, M.P., and Witt, P.J. (eds).CSIRO Publishing. 7 pp. http://www.cfd.com.au/cfd_conf15/PDFs/032JOH.pdf

Johansen, S.T. 1990. On the modelling of turbulent two phase flows. DrTechn thesis, Norwegian Institute of Technology, Trondheim.

Johansen, S.T. and Boysan, F. 1988. Fluid dynamics in bubble stirred ladles: Part II. Mathematical modeling. *Metallurgical Transactions B*, 19, 755–764.

Johansen, S.T., Meese, E.A., Zoric, J., I.slam, A., and Werner, M.D. 2017. On pragmatism in industrial modeling Part III: Application to operational drilling. *Progress in Applied CFD – CFD2017. Proceedings of the 12th International Conference on Computational Fluid Dynamics in the Oil & Gas, Metallurgical and Process Industries*. SINTEF, Trondheim, Norway. http://hdl.handle.net/11250/2465068

Kadkhodabeigi, M., Tveit, H., and Johansen, S.T., 2010. CFD modelling of the effect of furnace crater pressure on the melt and gas flows in the submerged arc furnaces used for silicon production. *Progress in Computational Fluid Dynamics*, 10, 374–383.

Launder, B.E. and Spalding, D.B. 1972. *Lectures in Mathematical Models of Turbulence*. Academic Press, London; New York.

Laux, H., Johansen, S.T., Berg, H., and Klevan, O.S., 2000. CFD analysis of the turbulent flow in ladles and the alloying process during tapping of stel furnaces. *Scandinavian Journal of Metallurgy*, 29, 71–80.

Morsi, S.A. and Alexander, A.J., 1972. An investigation of particle trajectories in two-phase flow system. *Journal of Fluid Mechanics*, 55, 193–208.

Zoric, J., Johansen, S.T., Einarsrud, K.T., and Solheim, A. 2014. On pragmatism in industrial modeling. *CFD 2014 - Proceedings of the 10th International Conference on Computational Fluid Dynamics in the Oil & Gas, Metallurgical and Process Industries*. Johansen, S.T. and Olsen, J.E. (eds). SINTEF, Trondheim. pp. 1–16.

Stein Tore Johansen
Principal Scientist, SINTEF
Adjunct Professor, NTNU

He received his M.Sc. in physics in 1981 and the Doctor of interest are multiphase physics, numerics and non-equilibrium thermodynamics, applied to industrial challenges in the metallurgical and oil & gas industries.
